The 9th European Congress on Computational Methods in Applied Sciences and Engineering
ECCOMAS Congress 2024
3–7 June 2024, Lisboa, Portugal

A NON-INTRUSIVE SURROGATE MODEL FOR HIP IMPLANT POSITIONING ECCOMAS CONGRESS 2024

Marlis Reiber[1,2], Fynn Bensel[1,3], Zhibao Zheng[1] and Udo Nackenhorst[1,2,3]

[1] Leibniz University Hannover
Institute of Mechanics and Computational Mechanics
Appelstraße 9a, Hannover, 30167, Germany
www.ibnm.uni-hannover.de

[2] Hannover Medical School
TRR 298: Safety Integrated and Infection Reactive Implants (SIIRI)
Carl-Neuberg-Straße 1, Hannover, 30625, Germany
www.siiri-sfb.de

[3] Leibniz University Hannover
International Research Training Group (IRTG) 2657
Appelstraße 11/11a, Hannover, 30167, Germany
www.irtg2657.uni-hannover.de

E-mails: marlis.reiber@ibnm.uni-hannover.de, fynn.bensel@ibnm.uni-hannover.de,
zhibao.zheng@ibnm.uni-hannover.de, nackenhorst@ibnm.uni-hannover.de

Key words: parametric surrogate model, proper orthogonal decomposition, radial basis functions, bone remodelling, mesh morphing, patient-specific simulation

Summary. A non-intrusive reduced order model combining proper orthogonal decomposition and radial basis function interpolation is introduced to evaluate the bone mass density change around hip implants for different implant positions. A reference finite element mesh is morphed using Laplace's equation. The mesh morphing maintains the total number of degrees of freedom and the node numbering which facilitates the usage of model order reduction techniques.

1 Introduction

According to the Australian Joint registry (2023), 4% of the primary total conventional hip arthroplasties require revision within 10 years [1]. The planning and monitoring of implants primarily rely on X-ray images [2, 3, 4]. Computational simulations of the bone remodelling process using the finite element method (FEM) can predict bone mass density (BMD) changes and, consequently, could provide additional information on the stability of the hip implant [5, 6]. Since the position of the implant is one of the most important factors for successful implantation [2], the aim is to develop a tool that enables fast predictions of BMD distributions for different implant positions, to help physicians in therapeutical decisions. Up-to-date, the computational effort of the current high-fidelity models is not feasible for the application in clinical practice [7, 5]. Reduced order models can be used to decrease the computational effort and enable fast

evaluations.
In the scope of this work, a non-intrusive surrogate model for the prediction of the BMD distribution for different implant positions is introduced. The model combines proper orthogonal decomposition (POD) with radial basis function (RBF) interpolation. The POD-RBF approach has been successfully applied in biomechanics, e.g. to analyse patient-specific hemodynamics [8, 9]. The setup of the surrogate model is divided in an offline and an online phase [10, 11].
In the offline phase, computationally expensive bone remodelling simulations are performed. A parameterised reference mesh is morphed to create the mesh for different implant positions. Mesh morphing maintains the total number of nodes and the node numbering which facilitates the usage of model order reduction techniques. Different mesh morphing techniques are available, e.g. using linear elasticity equation or Laplace's equation [12, 13]. In this work, Laplace's equation is employed. Subsequently, bone remodelling simulations are performed for different implant positions and the final BMD distribution is stored as snapshots. From these snapshots, the reduced basis are calculated using POD. In the online phase, a linear combination of the reduced basis and the weights, which are calculated using RBF interpolation, is used to quickly approximate the BMD solution for new implant positions.

2 Methods

2.1 Reference geometry

The reference FEM model with an integrated Metha® implant (Aesculap, Tuttlingen, Germany) is shown in Figure 1a and is morphed for different implant positions. The model as well as the boundary conditions, representing a clamping at the bottom and loading by the joint force as well as six muscle forces (see Figure 1b), are adopted from Lutz [14]. Further, the Gruen zones are defined on the reference mesh in Figure 1c.

2.2 Mesh morphing

Laplace's equation is used to morph the nodes of the parameterised reference mesh. The position of the implant is varied according to the parameters $\boldsymbol{\mu} = [\delta x, \delta y, \delta z, \alpha, \beta, \gamma]$ relative to the reference position ($\delta x = \delta y = \delta z = 0$ mm, $\alpha = \beta = \gamma = 0°$). $\delta_x, \delta_y, \delta_z$ are translations along and α, β, γ rotation angles around the x, y and z axes.
The mesh morphing via Laplace's equation is defined by

$$\Delta x_i(\boldsymbol{\mu}) = 0 \quad \text{where} \quad x_i = [x, y, z] \quad , \tag{1}$$

which is subject to the boundary conditions

$$\begin{cases} (x, y, z)|_{\Omega_1} & = (p, q, r)|_{\Omega_1} \\ (x, y, z)|_{\Omega_2} & = (g_x(\boldsymbol{\mu}), g_y(\boldsymbol{\mu}), g_z(\boldsymbol{\mu}))|_{\Omega_2} \end{cases} . \tag{2}$$

(p, q, r) are the initial nodal coordinates of the FEM model. The nodes of the boundary of the femur on Ω_1 remain fixed. The nodes of the implant and the cutting plane of the femur head on Ω_2 are performing a rigid body motion $(g_x(\boldsymbol{\mu}), g_y(\boldsymbol{\mu}), g_z(\boldsymbol{\mu}))$.

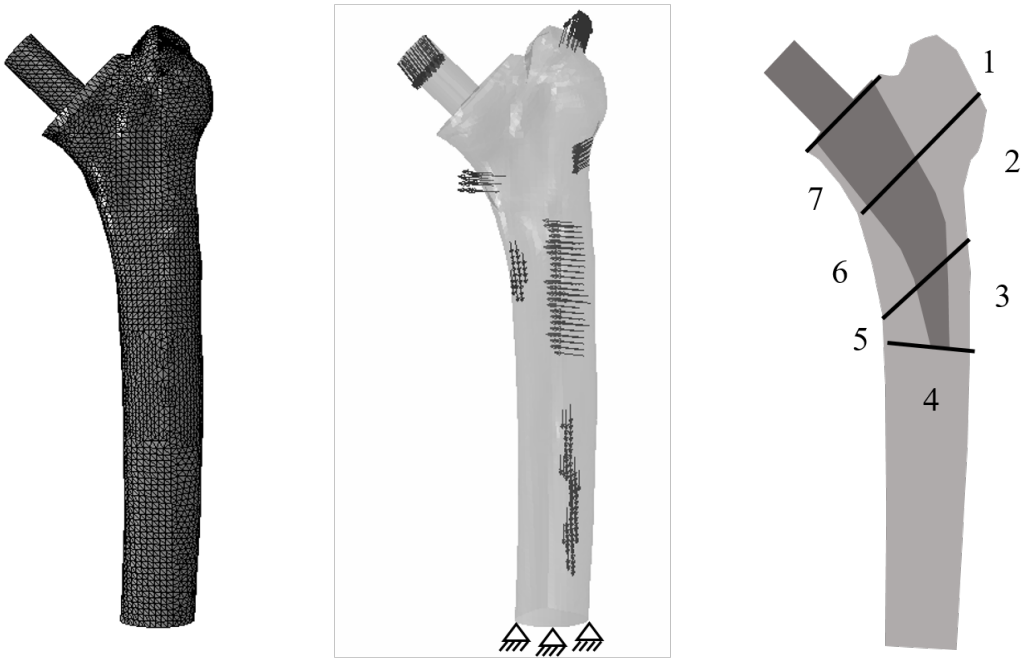

(a) Reference mesh (b) Boundary conditions (c) Gruen zones

s

Figure 1: FEM model with (a) reference mesh, (b) boundary conditions and (c) the Gruen zones for the reference mesh

The coordinates of the implant nodes performing the rigid body motion are calculated as

$$\begin{bmatrix} g_x(\boldsymbol{\mu}) \\ g_y(\boldsymbol{\mu}) \\ g_z(\boldsymbol{\mu}) \\ 1 \end{bmatrix} = \mathbf{T}(\boldsymbol{\mu}) \begin{bmatrix} p \\ q \\ r \\ 1 \end{bmatrix}_{\Omega_2} , \tag{3}$$

where $\mathbf{T}(\boldsymbol{\mu})$ is the transformation matrix, defined as

$$\mathbf{T}(\boldsymbol{\mu}) = \mathbf{R}_x\mathbf{R}_y\mathbf{R}_z\mathbf{D} = \begin{bmatrix} T_{11}(\boldsymbol{\mu}) & T_{12}(\boldsymbol{\mu}) & T_{13}(\boldsymbol{\mu}) & T_{14}(\boldsymbol{\mu}) \\ T_{21}(\boldsymbol{\mu}) & T_{22}(\boldsymbol{\mu}) & T_{23}(\boldsymbol{\mu}) & T_{24}(\boldsymbol{\mu}) \\ T_{31}(\boldsymbol{\mu}) & T_{32}(\boldsymbol{\mu}) & T_{33}(\boldsymbol{\mu}) & T_{34}(\boldsymbol{\mu}) \\ T_{41}(\boldsymbol{\mu}) & T_{42}(\boldsymbol{\mu}) & T_{43}(\boldsymbol{\mu}) & T_{44}(\boldsymbol{\mu}) \end{bmatrix} \begin{matrix} \rightarrow \mathbf{T}_x(\boldsymbol{\mu}) \\ \rightarrow \mathbf{T}_y(\boldsymbol{\mu}) \\ \rightarrow \mathbf{T}_z(\boldsymbol{\mu}) \\ \\ \end{matrix} . \tag{4}$$

$\mathbf{R}_x$, $\mathbf{R}_y$ and $\mathbf{R}_z$ are the rotation matrices around the corresponding axis and $\mathbf{D}$ is the translation matrix. Therefore, the x-coordinates of the implant nodes, here as an example for one node, are calculated as

$$g_x(\boldsymbol{\mu}) = \mathbf{T}_x(\boldsymbol{\mu}) \begin{bmatrix} p \\ q \\ r \\ 1 \end{bmatrix}_{\Omega_2} = \mathbf{T}_x(\boldsymbol{\mu})\mathbf{h}_{\Omega_2} . \tag{5}$$

Using the FEM to solve Laplace's equation results in the following system of equations

$$\begin{bmatrix} \mathbf{K}_{11} & \mathbf{K}_{12} & \mathbf{K}_{13} \\ \mathbf{K}_{21} & \mathbf{K}_{22} & \mathbf{K}_{23} \\ \mathbf{K}_{31} & \mathbf{K}_{32} & \mathbf{K}_{33} \end{bmatrix} \begin{bmatrix} \mathbf{x}_1(\boldsymbol{\mu}) \\ \mathbf{x}_2(\boldsymbol{\mu}) \\ \mathbf{x}_3(\boldsymbol{\mu}) \end{bmatrix} = \mathbf{0} \quad , \tag{6}$$

where $\mathbf{x}_1(\boldsymbol{\mu}) = \mathbf{p}_{\Omega_1}$ are the coordinates of the nodes on Ω_1 and $\mathbf{x}_2(\boldsymbol{\mu}) = \mathbf{G}_x(\boldsymbol{\mu}) = \mathbf{H}_{\Omega_2}^T \mathbf{T}_x^T(\boldsymbol{\mu})$ the coordinates of the nodes on Ω_2 performing the rigid body motion. $\mathbf{G}_x(\boldsymbol{\mu})$ and $\mathbf{H}_{\Omega_2}$ store the morphed and initial coordinates of the nodes on Ω_2.
In summary, the coordinates are calculated as

$$\mathbf{x}(\boldsymbol{\mu}) = \begin{bmatrix} \mathbf{p}_{\Omega_1} \\ \mathbf{H}_{\Omega_2}^T \mathbf{T}_x^T(\boldsymbol{\mu}) \\ -\mathbf{K}_{33}^{-1}\mathbf{K}_{31}\mathbf{p}_{\Omega_1} - \mathbf{K}_{33}^{-1}\mathbf{K}_{32}\mathbf{G}_x(\boldsymbol{\mu}) \end{bmatrix} = \begin{bmatrix} \mathbf{p}_{\Omega_1} & \mathbf{0} \\ \mathbf{0} & \mathbf{H}_{\Omega_2}^T \\ -\mathbf{K}_{33}^{-1}\mathbf{K}_{31}\mathbf{p}_{\Omega_1} & -\mathbf{K}_{33}^{-1}\mathbf{K}_{32}\mathbf{H}_{\Omega_2}^T \end{bmatrix} \begin{bmatrix} \mathbf{I} \\ \mathbf{T}_x^T(\boldsymbol{\mu}) \end{bmatrix}, \tag{7}$$

where $\mathbf{I}$ is the identity matrix. For the calculation of the new coordinates only $\mathbf{T}_x(\boldsymbol{\mu})$ needs to be recalculated. The remaining coordinate directions are treated analogously.

2.3 Bone remodelling simulation

For the bone remodelling simulation, a phenomenological model by Lutz and Nackenhorst [15] is used. From the constitutive relation of the BMD ϱ, introduced as an internal variable, and Young's modulus E

$$E = E_0 \left(\frac{\varrho}{\varrho_0} \right)^2 \quad , \tag{8}$$

where E_0 and ϱ_0 are reference values, the mechanical free energy density ψ_{mech} is defined as

$$\psi_{\text{mech}} = \left(\frac{\varrho}{\varrho_0} \right)^2 \psi^{\text{LE}} = \frac{1}{\varrho} \left(\frac{\varrho}{\varrho_0} \right)^2 \left[\frac{\lambda}{2} \text{tr}(\boldsymbol{\varepsilon})^2 + \mu \text{tr}(\boldsymbol{\varepsilon}^2) \right] \quad ,$$

where $\boldsymbol{\varepsilon}$ is the elastic strain, λ and μ are the Lamé parameters and ψ^{LE} is the linear elastic reference free energy.
The evolution equation for the BMD is defined as

$$\dot{\rho} = \frac{\partial \varrho}{\partial t} \quad , \tag{9}$$

where t denotes the process time of the quasi-static simulation. The BMD is limited by physiological limits of the minimum BMD ϱ_{min} and maximum BMD ϱ_{max}. Further, the mass source $\dot{\rho}$ is defined as

$$\dot{\rho} = c \left(\Psi - \Psi^{\text{ref}} \right) = c \left(\varrho\psi - \Psi^{\text{ref}} \right) \quad , \tag{10}$$

where c is a model parameter describing the speed of the remodelling process, Ψ the strain energy density and Ψ^{ref} represents a physiological target value.

2.4 Numerical treatment

The system of partial differential equations can be summarised as

$$\begin{cases} \nabla \cdot \boldsymbol{\sigma}\left(\boldsymbol{\varepsilon}, \varrho\right) = 0 & \text{in } \Omega \times \mathbb{T} \\ \quad \text{with } \boldsymbol{\varepsilon} = \nabla^{\mathrm{s}}\mathbf{u} & \\ \quad \text{and } \boldsymbol{\sigma} = \mathbb{C}\left(\varrho\right) : \boldsymbol{\varepsilon} & \\ \dot{\rho} = c\left(\Psi - \Psi^{\mathrm{ref}}\right) & \text{in } \Omega \times \mathbb{T} \end{cases} . \tag{11}$$

$\boldsymbol{\sigma}$ is the Cauchy stress, ∇^{s} is the symmetric gradient, Ω is the spatial domain and $\mathbb{T}$ is the process time domain.
The corresponding boundary and initial conditions are

$$\begin{cases} \mathbf{u} = \mathbf{u}_{\mathrm{D}} & \text{in } \partial\Omega_{\mathrm{D}} \times \mathbb{T} \\ \mathbf{n} \cdot \boldsymbol{\sigma} = \mathbf{t} & \text{in } \partial\Omega_{\mathrm{N}} \times \mathbb{T} \\ \varrho^{(0)} = \varrho_{\mathrm{init}} & \text{in } \Omega \times 0 \end{cases} . \tag{12}$$

$\partial\Omega_D$ is the Dirichlet boundary and $\partial\Omega_N$ is the Neumann boundary. $\mathbf{t}$ is the surface traction and $\mathbf{n}$ is the normal direction.
The FEM is used to solve the non-linear system of equations

$$\mathbf{K}(\mathbf{u})\Delta\mathbf{u} = \mathbf{f} \quad , \tag{13}$$

where $\mathbf{K}$ is the tangent stiffness matrix dependent on the displacements $\mathbf{u}$ and $\mathbf{f}$ is the non-equilibrium force vector. The Newton-Raphson method is used to solve the system of equations and the internal variable ϱ is updated using an implicit Euler scheme.
Further, a gradient enhancement approach is applied to the free energy

$$\Psi(\boldsymbol{\varepsilon}, \varrho, \phi) = \varrho\psi = \varrho\psi_{\mathrm{mech}}(\boldsymbol{\varepsilon}, \varrho) + \frac{\alpha_{\mathrm{GE}}}{2}(\phi - \varrho)^2 + \frac{\beta_{\mathrm{GE}}}{2} \mid \nabla\phi \mid^2 \quad , \tag{14}$$

where α_{GE} and β_{GE} are model parameters, and ϕ is the nodal representation of the BMD field [16].
The commercial software Abaqus (Abaqus 2017, Dassault Systèmes, Vélizy-Villacoublay, France) is used, along with a bone remodelling user element subroutine [17]. The parameter values are summarised in Table 1. The biomechanically equilibrated BMD distribution for the complete femur is projected onto the model with the implant to get the initial distribution. For the implant, titanium is used as linear elastic material with a Young's modulus $E = 105000\ \mathrm{N/mm^2}$ and a Poisson's ratio $\nu = 0.3$. In Figure 2, the initial and final BMD distribution for the reference mesh are shown, depicting a decreasing BMD distribution in Gruen zone 7.

2.5 Surrogate model

The POD-RBF surrogate model is set up to approximate the full BMD solution $\boldsymbol{\phi}$ for a new set of parameters $\boldsymbol{\mu}$ as a linear combination of reduced basis functions $\mathbf{V}$ and the corresponding weights $\boldsymbol{w}(\boldsymbol{\mu})$

$$\boldsymbol{\phi} \approx \tilde{\boldsymbol{\phi}} = \mathbf{V} \cdot \boldsymbol{w}(\boldsymbol{\mu}) \quad . \tag{15}$$

Table 1: Bone remodelling simulation parameters

Parameter	**Value**	**Unit**
E_0	6500.0	[N/mm^2]
ν	0.3	[-]
ϱ_0	1.0	[g/cm^3]
Ψ_{ref}	0.002	[N/mm^2]
c	0.01	[s/m^2]
ϱ_{min}	0.001	[g/cm^3]
ϱ_{max}	2.0	[g/cm^3]
α_{GE}	0.01	[m^5/s^{2}kg]
β_{GE}	10^{-8}	[m^7/s^{2}kg]

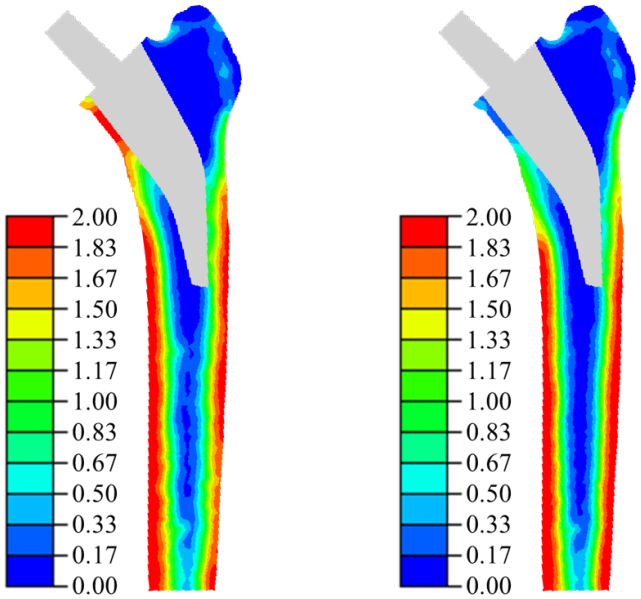

(a) Initial BMD distribution (b) Final BMD solution

Figure 2: Initial (a) and final (b) BMD distribution (ϕ in g/cm^3) for reference position of hip implant

2.5.1 Proper orthogonal decomposition

The reduced basis functions $\mathbf{V}$ in Equation (15) are calculated using POD. n_s high-fidelity simulations are performed at different parameter points. The BMD distribution $\boldsymbol{\phi}_i = \boldsymbol{\phi}(\boldsymbol{\mu}_i)$ represents the i^{th} solution with the corresponding parameter vector $\boldsymbol{\mu}_i$. These solution snapshots are collected in the snapshot matrix $\mathbf{S} = [\boldsymbol{\phi}_1, \cdots, \boldsymbol{\phi}_{n_s}] \in \mathbb{R}^{N \times n_s}$ where N is the number of nodes.

The matrix decomposition of $\mathbf{S}$, using singular value decomposition (SVD), is performed

$$\mathbf{S} = \mathbf{U}\boldsymbol{\Sigma}\mathbf{Z}^T \quad , \tag{16}$$

where $\mathbf{U} = [\boldsymbol{\xi}_1, \cdots, \boldsymbol{\xi}_N] \in \mathbb{R}^{N \times N}$ and $\mathbf{Z} = [\boldsymbol{\zeta}_1, \cdots, \boldsymbol{\zeta}_{n_s}] \in \mathbb{R}^{n_s \times n_s}$ are matrices containing the left and right singular vectors and $\mathbf{Z} = \text{diag}(\varsigma_1, \cdots, \varsigma_{n_s}) \in \mathbb{R}^{N \times n_s}$ is a matrix containing the singular values of $\mathbf{S}$, where $\varsigma_1 \geq \cdots \geq \varsigma_{n_s} \geq 0$.
The POD modes $\mathbf{V} = [\boldsymbol{\xi}_1, \cdots, \boldsymbol{\xi}_n]$ are a subset of $\mathbf{U}$ comprising the n left singular vectors corresponding to the n largest singular values, thereby capturing a predefined amount of the "relative" energy [10, 11].

2.5.2 Radial basis function interpolation

RBF interpolation is used to calculate the weights in Equation (15) as

$$\boldsymbol{w}(\boldsymbol{\mu}) = \sum_{i=1}^{n_s} \boldsymbol{\omega}_i \varphi(r) \quad , \tag{17}$$

where $\boldsymbol{\omega}_i$ are the RBF coefficients to be determined and $\varphi(\cdot)$ is the RBF. Different kernel functions can be used as an RBF. In this work, the Matérn C^0 RBF $\phi(r) = e^{-a \cdot r}$ is used. $r = \|\boldsymbol{\mu} - \boldsymbol{\mu}_i\|$ is the radial distance where $\|\cdot\|$ denotes the Euclidean norm. All parameter inputs are normalised.
The coefficients can be determined by solving

$$\mathbf{A} = \mathbf{S}_r \mathbf{B}^{-1} \quad , \tag{18}$$

where $\mathbf{A} \in \mathbb{R}^{n \times n_s}$ contains the coefficient vectors $\mathbf{A} = [\boldsymbol{\omega}_1, \cdots, \boldsymbol{\omega}_{n_s}]$, $\mathbf{S}_r$ is the reduced snapshot matrix with the known data and $\mathbf{B} \in \mathbb{R}^{n_s \times n_s}$ is the interpolation matrix evaluating the RBFs at all parameter combinations $\mathbf{B} = [\mathrm{B}_{ij}] = [\varphi(\|\boldsymbol{\mu}_i - \boldsymbol{\mu}_j\|)]$ with $i, j = 1, \ldots, n_s$.

3 Numerical example

3.1 Setup of surrogate model

An equidistant sampling with three points in every parameter dimension in the range of $\delta x, \delta y, \delta z \in [-1, 1]$ mm and $\alpha, \beta, \gamma \in [-1, 1]^\circ$ is performed. The bone remodelling simulation is performed on all 729 morphed reference meshes and the final result of $\boldsymbol{\phi}$ combined with the parameter combination $\boldsymbol{\mu}$ is stored.
For the setup of the surrogate model, 17 POD modes are selected as the reduced basis which preserves a total energy of 99.99%. For the RBF, a shape parameter of $a = 0.0001$ is chosen.
For the computations, a workstation Intel(R) Core(TM) i7-6700 CPU @ 3.40GHz with 32GB RAM was used. The time for the mesh generation in the offline phase is 6 minutes and each bone remodelling simulation takes about 25 minutes. The time to set up the surrogate model, including the calculation of the POD modes and the RBF coefficients, takes approximately 2.7 seconds. The time to calculate a new parameter point in the online stage is about 1.2 milliseconds. The calculation of the parameterised mesh takes 0.4 seconds.
To analyse the accuracy of the surrogate model, 20 pseudo random parameter points in the parameter range are created.

3.2 Results

The mean absolute error (MAE) for the validation set is 0.0047. In Table 2, the MAE is depicted for the different Gruen zones. The MAE is the smallest in Gruen zone 4, with a value of 0.0006. In Gruen zone 4, the mass change is the smallest, so changes in the BMD distribution are small between different parameter combinations and are easily represented by the chosen POD modes. In contrast, in Gruen zone 7, the largest error with 0.0214 is present. In Gruen zone 7, the largest mass change is present, which needs to be captured by the POD modes.

Table 2: Mean absolute error in different Gruen zones for POD-RBF surrogate model

Gruen zone	MAE
1	0.0050
2	0.0046
3	0.0088
4	0.0006
5	0.0049
6	0.0083
7	0.0214

In Figure 3, the results for the high-fidelity solution, the surrogate model solution and the absolute error for one exemplary random position ($\delta_x = 0.99$ mm, $\delta_y = 0.35$ mm, $\delta_z = -0.54$ mm, $\alpha = -0.34°$, $\beta = -0.74°$ and $\gamma = 0.84°$) are shown. Qualitatively, no difference between the BMD distributions of the high-fidelity model and the surrogate model is visible. The MAE for a cut through the femur is depicted in Figure 3c. A maximum error of 0.15 is present but smaller errors occur in the vicinity.

4 Conclusions

A non-intrusive POD-RBF reduced order model has been implemented to quickly evaluate various hip implant positions. Using a mesh morphing approach, remeshing can be avoided in the offline phase. Further, the node numbering is maintained which prevents the need for projection of the results on a common mesh in the offline and online phase. By using the surrogate model, the computational time for new parameter points can be significantly reduced compared to the high-fidelity model, while still maintaining a good accuracy. This time reduction paves the way for application of the surrogate model in clinical practice.

5 Acknowledgements

M. Reiber is funded by the DFG through the SFB/TRR-298-SIIRI – Project-ID 426335750. F. Bensel is funded by the DFG through the IRTG 2657 grant 433082294. Z. Zheng is funded by the DFG through Grant Number 527222589.

REFERENCES

[1] Smith, P.N., Gill, D.R., McAuliffe, M.J., McDougall, C., Stoney, J.D., Vertullo, C.J., Wall, C.J., Corfield, S., Page, R., Cuthbert, A.R., Du, P., Harries, D., Holder, C., Lorimer, M.,

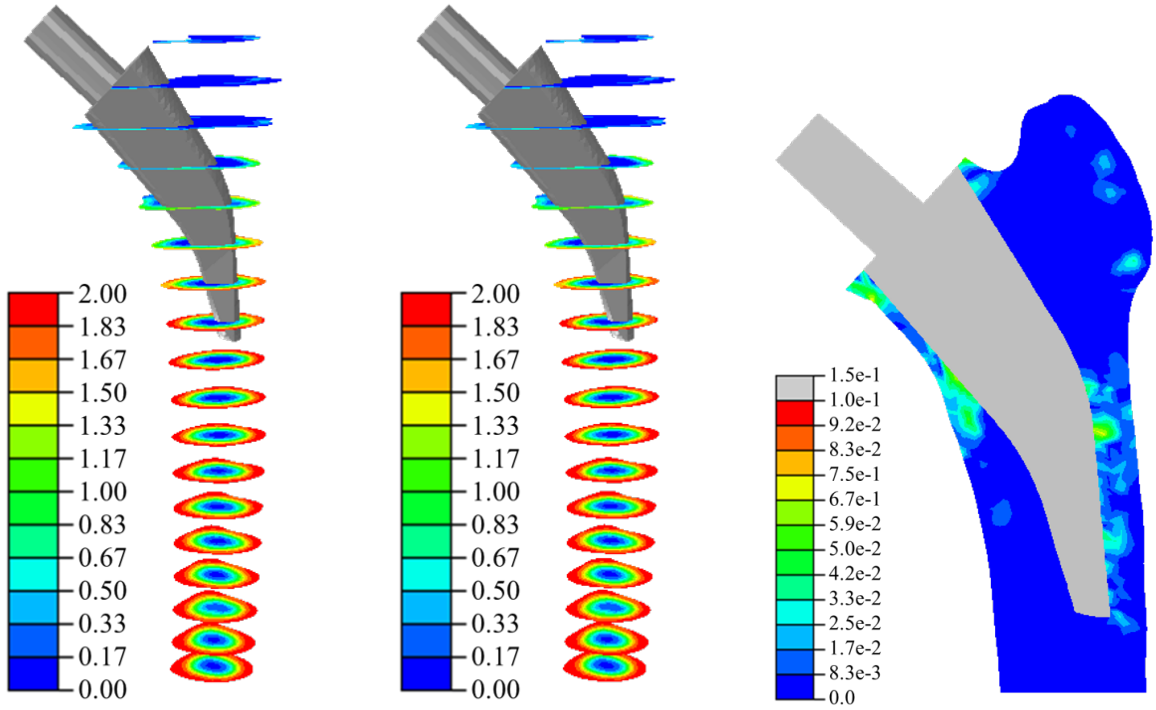

(a) High-fidelity solution (b) Surrogate model solution (c) Absolute error

Figure 3: Exemplary results for final BMD ϕ distribution in g/cm^3 for a random implant position ($\delta_x = 0.99$ mm, $\delta_y = 0.35$ mm, $\delta_z = -0.54$ mm, $\alpha = -0.34°$, $\beta = -0.74°$ and $\gamma = 0.84°$) (a) high-fidelity solution (b) surrogate model solution (c) absolute error

Cashman, K., Lewis, P.: Hip, Knee & Shoulder Arthroplasty: 2023 Annual Report (2023). https://doi.org/10.25310/YWQZ9375

[2] Floerkemeier, T.: Patientenspezifische Planung in der Hüftendoprothetik. Arthroskopie **34**, 377–384 (2021). https://doi.org/10.1007/s00142-021-00461-y

[3] Roth, T.D., Maertz, N.A., Parr, J.A., Buckwalter, K.A., Choplin, R.H.: CT of the hip prosthesis: appearance of components, fixation, and complications. Radiographics **32**(4), 1089–1107 (2012). https://doi.org/10.1148/rg.324115183

[4] Miller, T.T.: Imaging of hip arthroplasty. European Journal of Radiology **81**(12), 3802–3812 (2012). https://doi.org/10.1055/s-2006-934215

[5] Nackenhorst, U.: Modeling of bone adaption processes. In: Altenbach, H., Öchsner, A. (eds.) Encyclopedia of Continuum Mechanics, pp. 1–11. Springer, Berlin Heidelberg (2018). https://doi.org/10.1007/978-3-662-53605-6_33-1

[6] Sun, X., Curreli, C., Viceconti, M.: Finite element models to predict the risk of aseptic loosening in cementless femoral stems: A literature review. Applied Sciences **14**(8) (2024). https://doi.org/10.3390/app14083200

[7] Webster, D., Müller, R.: In silico models of bone remodeling from macro to nano—from organ to cell. Wiley Interdisciplinary Reviews: Systems Biology and Medicine **3**(2), 241–251 (2011). https://doi.org/10.1002/wsbm.115

[8] Girfoglio, M., Ballarin, F., Infantino, G., Nicoló, F., Montalto, A., Rozza, G., Scrofani, R., Comisso, M., Musumeci, F.: Non-intrusive PODI-ROM for patient-specific aortic blood flow in presence of a LVAD device. Medical Engineering & Physics **107**, 103849 (2022). https://doi.org/10.1016/j.medengphy.2022.103849

[9] Balzotti, C., Siena, P., Girfoglio, M., Stabile, G., Dueñas-Pamplona, J., Sierra-Pallares, J., Amat-Santos, I., Rozza, G.: A reduced order model formulation for left atrium flow: an atrial fibrillation case. Biomechanics and Modeling in Mechanobiology, 1–19 (2024). https://doi.org/10.1007/s10237-024-01847-1

[10] Quarteroni, A., Manzoni, A., Negri, F.: Reduced Basis Methods for Partial Differential Equations: an Introduction vol. 92. Springer, Berlin Heidelberg (2015). https://doi.org/10.1007/978-3-319-15431-2

[11] Chinesta, F., Huerta, A., Rozza, G., Willcox, K.: Model Reduction Methods. In: Stein, E., Borst, R., Hughes, T.J.R. (eds.) Encyclopedia of Computational Mechanics, 2nd edn., pp. 1–36. John Wiley & Sons, Ltd, Hoboken, New Jersey (2017). Chap. 2. https://doi.org/10.1002/9781119176817.ecm2110

[12] Bah, M.T., Nair, P.B., Browne, M.: Mesh morphing for finite element analysis of implant positioning in cementless total hip replacements. Medical Engineering & Physics **31**(10), 1235–1243 (2009). https://doi.org/10.1016/j.medengphy.2009.08.001

[13] Zheng, Z., Valdebenito, M., Beer, M., Nackenhorst, U.: Simulation of random fields on random domains. Probabilistic Engineering Mechanics **73**, 103455 (2023). https://doi.org/10.1016/j.probengmech.2023.103455

[14] Lutz, A.: Ein integrales Modellierungskonzept zur numerischen Simulation der Osseointegration und Langzeitstabilität von Endoprothesen. PhD thesis, Gottfried Wilhelm Leibniz University, Hannover (2011)

[15] Lutz, A., Nackenhorst, U.: Numerical investigations on the biomechanical compatibility of hip-joint endoprostheses. Archive of Applied Mechanics **80**(5), 503–512 (2010). https://doi.org/10.1007/s00419-009-0380-4

[16] Bensel, F., Reiber, M., Foulatier, E., Junker, P., Nackenhorst, U.: A gradient-enhanced bone remodelling approach to avoid the checkerboard phenomenon. Computational Mechanics, 1–15 (2023). https://doi.org/10.1007/s00466-023-02413-9

[17] Bensel, F., Reiber, M.: A gradient-enhanced bone remodelling approach to avoid the checkerboard phenomenon. LUIS. https://doi.org/10.25835/TH2MQZOM (2022). https://doi.org/10.25835/TH2MQZOM